Analysis of ^{31}P nuclear magnetic resonance lineshapes and transversal relaxation of bacteriophage M13 and tobacco mosaic virus

Pieter C. M. M. Magusin and Marcus A. Hemminga
Department of Molecular Physics, Agricultural University, Dreyenlaan 3, 6703 HA Wageningen, The Netherlands

ABSTRACT The experimentally observed ^{31}P lineshapes and transversal relaxation of 15% (wt/wt) M13, 30% M13, and 30% tobacco mosaic virus (TMV) are compared with lineshapes and relaxation curves that are simulated for various types of rotational diffusion using the models discussed previously (Magusin, P. C. M. M., and M. A. Hemminga. 1993. Biophys. J. 64:1851–1860). It is found that isotropic diffusion cannot explain the observed lineshape effects. A rigid rod diffusion model is only successful in describing the experimental data obtained for 15% M13. For 30% M13 the experimental lineshape and relaxation curve cannot be interpreted consistently and the TMV lineshape cannot even be simulated alone, indicating that the rigid rod diffusion model does not generally apply. A combined diffusion model with fast isolated motions of the encapsulated nucleic acid dominating the lineshape and a slow overall rotation of the virion as a whole, which mainly is reflected in the transversal relaxation, is able to provide a consistent picture for the 15 and 30% M13 samples, but not for TMV. Strongly improved lineshape fits for TMV are obtained assuming that there are three binding sites with different mobilities. The presence of three binding sites is consistent with previous models of TMV. The best lineshapes are simulated for a combination of one mobile and two static sites. Although less markedly, the assumption that two fractions of DNA with different mobilities exist within M13 also improves the simulated lineshapes. The possible existence of two ^{31}P fractions in M13 sheds new light on the nonintegral ratio 2.4:1 between the number of nucleotides and protein coat subunits in the phage: 83% of the viral DNA is less mobile, suggesting that the binding of the DNA molecule to the protein coat actually occurs at the integral ratio of two nucleotides per protein subunit.

INTRODUCTION

Bacteriophage M13 has a cylindrical shape with a length of ~900 nm and a varying outer diameter between 6 and 10 nm depending on the relative humidity (1, 2). The molecular mass of the phage is ~16 MD. Its genome is a circular single-stranded DNA molecule of 6,407 nucleotides (3) protected by a protein coat mainly consisting of ~2,700 copies of the gene-8 protein. The DNA molecule is situated along the virion in a core of <2.5 nm wide. Studies by x-ray fiber diffraction applied to bacteriophage fd, which is closely related to M13, indicate that the symmetry of the protein coat involves a five-fold axial rotation axis combined with a two-fold axial screw axis of pitch 32 Å (4). Much less is known about the geometry of the encapsulated DNA molecule. The absence of DNA reflections in earlier reported x-ray patterns has led to the conclusion that the molecule is mobile or disordered (5), but later results show that some regular DNA structured with a pitch of 27 Å may exist and that many of the bases are stacked axially ~3.4 Å apart (4). Substantial base stacking is detected by ultraviolet (UV) spectroscopy as well (6), but the distance of 3.4 Å is difficult to reconcile with the mean axial rise of 2.7 Å expected for homogeneous distribution of DNA along the inside of the protein coat, as commonly assumed (4, 7). Raman spectra of fd contain the characteristics of nucleoside sugar pucker and glycosyl torsion typical for A-DNA. However, only 20% of the viral DNA at most seems to have the regular phosphodiester backbone found in A-DNA (8). In fact, infrared linear dichroism results indicate that the DNA backbone mainly has a B-type conformation (9). Phosphorus solid state nuclear magnetic resonance (NMR) studies applied to bacteriophage fd have indicated that the DNA within the virion is relatively immobile (10), probably as a consequence of the electrostatic interaction between the negatively charged phosphodiesters in the DNA to the positively charged lysine residues located on the inside of the tubular protein coat. There are no signs for any regularity in the DNA structure present in the spectra of oriented fd gels (11). The motional narrowing of the phosphorus lineshape observed for unoriented and oriented fd gels has been interpreted qualitatively in terms of both rotational diffusion of the virion as a whole around its length axis (10) and limited motions present in the DNA backbone (11).

Tobacco mosaic virus (TMV) is a rod-shaped single-stranded RNA virus with a length of 3,000 Å and an outer diameter of 180 Å. The protein coat is formed by 2,200 subunits (M_r = 17,500) arranged in a helix with 49 subunits per three turns. In contrast to the DNA molecule in fd, the structure of the RNA molecule, which consists of 6,600 nucleotides, has been well determined. It is buried within the coat between layers of subunits, following the protein helix with three nucleotides per protein subunit at a radius of ~40 Å (12). Three sorts of binding between RNA and protein subunits inside TMV have been suggested: electrostatic interactions between phosphodiesters and arginine residues, hydrophobic interactions between the nucleotide bases and the left radial α-helix of the subunits, and hydrogen bridges (13).

Address correspondence to M. A. Hemminga, Department of Molecular Physics, Agricultural University, P. O. Box 8128, 6700 ET Wageningen, The Netherlands.

As a consequence of the regular RNA geometry, three types of phosphorus nuclei can be distinguished in NMR spectra of oriented TMV samples and in magic angle spinning (MAS) NMR spectra of TMV. The three phosphorus resonances in the spectrum of oriented TMV samples have different linewidths that have been assigned to varying degrees of disorder in the orientation of the phosphates in the various binding sites of the coat protein (14). In MAS spectra of TMV, two lines strongly overlap indicating similar electronic environments for two of three binding sites (14, 15).

To gain information about the dynamic behavior of the nucleic acid backbone in M13 and TMV, we used ^{31}P solid state NMR spectroscopy. In a previous report we demonstrated how isotropic diffusion and various types of uniaxial diffusion influence ^{31}P NMR lineshapes and transversal relaxation theoretically (16). Here we will compare the experimental NMR results with the outcome of these simulations.

MATERIALS AND METHODS

Preparation and purification of M13 and TMV

M13 bacteriophage was grown and purified as described by Spruijt et al. (17) except for 10 mM Tris, 0.2 mM EDTA being used as the final dialyzing and storage buffer. TMV was prepared as described previously (15). Gels containing 30% (wt/wt) TMV or up to 20% M13 were directly obtained from the storage suspensions by centrifugating for 4 h in a Ti-75 rotor (model Ti-75; Beckman Instruments, Inc., Palo Alto, CA) at 55,000 rpm. To prepare gels containing more M13, wet M13 pellets were concentrated further by drying. Finally, the wet pellets were spread out on the inside of the centrifuge tube and the material was dried under a flow of air during 2–8 h at slightly below room temperature. For maximal homogeneity of humidity within the pellets, the material was repelleted at low speed and spread out again on the inside of the centrifuge tube several times during the drying procedure. The change of water content in the drying pellets was roughly followed by weighing and finally determined by measuring the phage concentration spectrophotometrically using $A_{260} = 3.80$ (0.1% wt/vol, 1-cm path length) for M13 and $A_{260} = 3.00$ for TMV. Samples were prepared ≥ 12 h before the NMR experiments and were stored at 4°C.

NMR methods

NMR spectra were recorded on a spectrometer (model CXP300; Bruker Instruments, Inc., Billerica, MA) operating at a ^{31}P NMR frequency of 121.5 MHz. Because of the dielectric properties of wet M13 and TMV gels, the $\pi/2$ pulse was carefully set to 5 μs on the weak ^{31}P signal of the sample itself. For cross-polarization experiments, the Hartmann–Hahn condition was found by measuring the ^{1}H $\pi/2$ pulse length directly on the water signal and setting it equal to the ^{31}P $\pi/2$ pulse length. In all experiments a CYCLOPS phase alternation was used to remove the effects of pulse imperfections and high power proton decoupling was on during refocussing delays and acquisition time.

Sample tubes were sealed with glue to keep the water content in the gel constant. This was checked by comparing the sample weight before and after the experiments. Temperature was controlled by a temperature unit (Bruker Instruments, Inc.) connected to a thermocouple positioned at a 3-cm distance from the sample coil. This system was calibrated using an 1010 fluoroptic thermometer (model 1010; ASEA, Västerås, Sweden). The glass fiber detection probe of this instrument does not contain electronic parts and therefore functions correctly in strong electromagnetic fields, so that the temperature can be measured inside the sample during the actual pulse experiment. The fluoroptic thermometer could only be used for calibration, because sample tubes could not be sealed completely with the temperature fiber penetrating through the tube cap. Substantial differences were observed between the indication of the fluoroptic thermometer and the Bruker unit, especially below room temperature, because a temperature gradient existed within the probehead between the sample directly cooled by a flow of nitrogen and the probewall heated by the surrounding shimming coils. The fluoroptic thermometer also showed that the immediate heating effect by high power decoupling was much stronger than estimated from the steady state indication of the temperature unit (Bruker Instruments, Inc.).

Spectra were recorded using cross-polarization and a Hahn echo pulse sequence to remove the effect of probe ringing on the weak signal. For recording standard spectra the echo was made to occur 60 μs after excitation. Transversal relaxation was studied by acquiring the Hahn echoes for a series of refocussing delays and analyzing them in a powder average way by fitting an exponential curve to the echo decay directly. Longitudinal relaxation was determined using the direct inverse recovery pulse sequence, followed by curve fitting applied to the spectra after Fourier transformation. Because in M13 gels ^{31}P longitudinal relaxation is much slower than transversal relaxation, it was possible to develop a T_1-filtered T_2 experiment by combining the Carr–Purcell–Meiboom–Gill (CPMG) experiment for the T_2 measurement (18) and the progressive saturation method for the T_1 measurement. This enabled us to investigate a possible correlation between longitudinal and transversal relaxation in M13 gels (19, 20). The pulse spacing in the CPMG sequence was set to 650 μs, because spinlocking effects occurred at smaller pulse interspacing. At the end of the acquisition time of 20 ms an additional $\pi/2$ pulse was given to reduce longitudinal magnetization effects due to pulse imperfections. The repetition time was varied from 2 to 24 s.

Simulation procedures

Phosphorus NMR lineshapes and powder average transversal relaxation decays at 121.5 MHz have been simulated for isotropic, uniaxial, and combined diffusion using self-made Fortran programs as described previously (16). For ^{31}P NMR in M13, relative chemical shift tensor values $\sigma_{xx} - \sigma_o = 77$ ppm, $\sigma_{yy} - \sigma_o = 18$ ppm, and $\sigma_{zz} - \sigma_o = -95$ ppm were taken (where σ_o is the isotropic shift), as obtained from analysis of sideband intensities in several MAS spectra of dehydrated and frozen samples recorded at 202.5 MHz. These values correspond within experimental error to the values reported for bacteriophage fd, which is closely related to M13 (10). For TMV the values 83, 25, and −108 ppm were taken from the literature (14). In simulations for M13 it was assumed that a random distribution of shift tensor orientations exists within the phage, much like the random orientations of microcrystallites within a MAS spinner. For TMV the orientation of ^{31}P shift tensor for the three different binding sites with respect to the rod-shaped TMV was approximately derived from the ^{31}P atomic coordinates (13), assuming that in phosphodiesters the σ_{yy} lies in the direction of the bisector of the O-P-O angle (as opposed to the RO-P-OR′ angle) and that σ_{zz} lies in the O-P-O plane, as well (21). From these approximate tensor orientations (β_i, γ_i) the chemical shift values of the three ^{31}P NMR lines in the spectrum of an oriented sample of TMV were calculated. By comparing these shift values with the ones calculated earlier (14), we found that sites 1, 2, and 3 as labeled by Stubbs and Stauffacher (13) probably correspond to the lines A, C, and B, respectively, according to the labeling by Cross et al. (14). Because the calculated shift values differ from the experimentally observed ones (14), we slightly modified the angles β_i such that the three ^{31}P lines shifted to the observed positions in the spectrum of oriented TMV without changing their frequency order. These modified angles β_i and the unchanged angles γ_i were used to define the orientation of ^{31}P tensors within TMV (Table 1). The best fits to the experimental lineshapes of M13 and TMV were found by a least-square fitting, allowing height, baseline, and isotropic

TABLE 1 **Labeling of the three binding sites in TMV in different papers and the orientation of the three shift tensors with respect to the axis of TMV as calculated from model coordinates* and refined from the shift in the oriented spectrum‡**

Label							
Ref. 13	Ref. 12	Ref. 14	Calculated β	Calculated γ	Calculated σ	Observed σ‡	Refined β
			rad		*ppm*		*rad*
1	2	A	0.85	1.21	−29.2	+27	1.03
2	1	C	0.63	0.81	−51.9	0	0.93
3	3	B	0.48	1.02	−76.6	−25	0.75

* Reference 13.
‡ Reference 14.

shift of simulated lineshapes to vary. Simulated transversal relaxation curves were fitted to the experimental relaxation decays with only height as a variable.

RESULTS

The ^{1}H decoupled ^{31}P NMR spectra of samples of 15 and 30% (wt/wt) M13 and 30% (wt/wt) TMV at 121.5 (Fig. 1 *a*) and at 202.5 MHz (not shown) show the characteristic lineshape caused by chemical shift anisotropy (CSA). From these spectra the difference between the largest and the smallest CSA tensorvalue $|\sigma_{zz} - \sigma_{xx}|$ can be directly estimated as 170 ppm for M13 and 190 ppm for TMV. Lineshape discontinuities are only partially defined in the spectra of M13 and TMV gels. The powder average decays of ^{31}P NMR Hahn echoes fit well to single exponentials for the two M13 samples and reasonably for TMV (Fig. 2 *a*). In this way, transversal relaxation times T_{2e} of 0.39, 0.79, and 1.5 ms are found for ^{31}P in 15, and 30% M13 and 30% TMV gels, respectively. The results above have been obtained using cross-polarization, but no significant differences in lineshapes or relaxation rates are observed when direct excitation is used.

To gain more information about the mechanism causing transversal relaxation, M13 gels have been studied at various frequencies, concentrations, and temperatures.

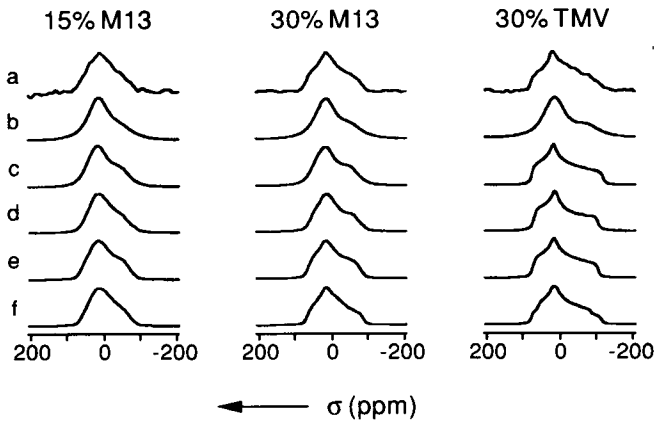

FIGURE 1 Experimental and simulated ^{31}P lineshapes obtained for 15% (wt/wt) M13 (*left;* 2,560 scans), 30% M13 (*middle;* 768 scans), and 30% TMV (*right;* 512 scans). Experimental spectra (*a*) are obtained by Fourier transformation of the echo at 60 μs created by a π pulse of 10 μs centered at 30 μs; best-fitting lineshapes by Fourier transformation of echoes (*b*) and free induction decays (*c*) simulated for isotropic diffusion; best echo simulated for rigid rod diffusion (*d*); best echo simulated for combined diffusion (*e*); best echo simulated for combined diffusion with two (*left* and *central* columns) or three (*right* column) internal components; for diffusion coefficients and restriction halfangles see text.

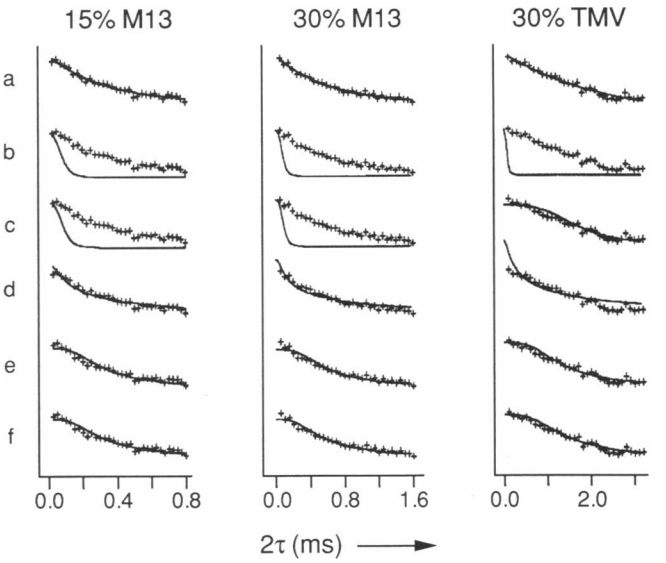

FIGURE 2 Experimental (*a*) and simulated (*b–f*) ^{31}P transversal relaxation decays for 15% M13 (*left*) 30% M13 (*middle*), and 30% TMV (*right*); for 15% M13 32 echoes were measured at subsequent multiples of 25 μs starting at 25 μs, including the finite pulse length of 10 μs (*left, a*); for 30% M13 32 echoes were measured at subsequent multiples of 50 μs starting at 50 μs (*center, a*); for 30% TMV 32 echoes were measured at subsequent multiples of 100 μs starting at 200 μs (*right, a*); decay for best Fourier-transformed echo (*b*) and FID (*c*) simulated for isotropic diffusion; best decay simulated for rigid rod diffusion (*d*), best decay simulated for combined diffusion (*e*), best decay simulated for combined diffusion with two (*left* and *middle, f*) or three (*right, f*) internal components; for diffusion coefficients and restriction halfangles see text.

In these studies it was generally observed that T_{2e} times, obtained by single-exponential fitting, decrease with magnetic field strength and increase with decreasing temperature and hydration, i.e., with increasing sample viscosity. Proton-decoupled T_{2e} values measured for gels of M13 in D_2O, are shorter than the corresponding values measured for equally concentrated gels in H_2O. This is presumably due to static $^2H-^{31}P$ dipolar interactions, which could not be eliminated in our experiments. In contrast to T_{2e}, the longitudinal relaxation time T_1 does not vary significantly for M13 concentrations between 10 and 40% (wt/wt) and temperatures between 10 and 40°C. In this range of concentrations and temperatures, an average T_1 value of 4.0 ± 0.4 s is measured at 121.5 MHz. Only at low hydration T_1 becomes larger, e.g., 8 s for 80% M13. The large difference between T_1 and T_2 makes it possible to carry out hybrid relaxation experiments. It is found in these experiments that the transversal relaxation time T_2^{CP}, measured from the decay of CPMG echoes, is roughly independent of the repetition rate and that the longitudinal relaxation time is approximately the same for all the CPMG echoes. Thus, no T_1 filtering effect on T_2^{CP}, nor T_2^{CP} filtering effect on T_1 is detectable. Transversal relaxation rates as obtained from the decay of CPMG echoes in our hybrid experiments do not differ significantly from the rates observed in the Hahn echo decay for the pulse interspacing (650 μs) used. If the pulse interspacing is decreased, however, T_2^{CP} becomes longer.

DISCUSSION

The width of the observed ^{31}P NMR line and its proportionality to the magnetic field provide strong evidence for CSA being the dominant line-broadening factor in ^{31}P spectra of M13 and TMV gels. Because line discontinuities characteristic for static CSA are only partially defined in the experimental spectra, other influences on the lineshape should be considered as well. As no protons are directly bound to ^{31}P in the nucleic acid backbone, the high power proton decoupling used is sufficient to remove heteronuclear dipolar broadening from the spectra completely. The large distance between subsequent phosphorus nuclei of about 6–7 Å in TMV and presumably in M13 as well (13, 22) and the low gyromagnetic ratio of phosphorus nuclei, rule out the possibility that homonuclear dipolar coupling has a strong effect on the ^{31}P resonance line. This finally leaves motional narrowing as the most likely explanation for the absence of sharp line discontinuities. Indeed, in M13 spectra the narrowing effect appears more pronounced at high hydration (Fig. 1).

In contrast to their effect on the lineshape, hydration and temperature strongly influence transversal relaxation of phosphorus nuclei in M13. For example, as hydration decreases from 85 to 70%, T_{2e} doubles from 0.39 to 0.79 ms. Because at higher hydration and temperature more motion is probably present in M13 gels, T_{2e} aptrend expected from Redfield theory. The value of T_{2e} of 1.5 ms found for TMV suggests that ^{31}P mobility in 30% TMV gels is less than in M13 gels at a comparable hydration percentage. Several transversal relaxation mechanisms can be considered to explain this effect. High power decoupling, as used in our experiments, is sufficient to remove static $^1H-^{31}P$ dipolar coupling effects from the transversal relaxation decay, as was tested by varying the decoupling power. It does not, however, eliminate the relaxating influence of highly mobile water protons in the vicinity of ^{31}P. T_2 experiments in D_2O to evaluate this solvent effect suffer from the difficulty that deuterons exchange with protons in the virion and thereby cause static $^2H-^{31}P$ dipolar effects, which cannot be removed unless deuterons are decoupled at a third frequency. In principle, the observed T_{2e} increase at decreasing hydration could indeed result from the removal of mobile water protons close to ^{31}P. For motions with such short correlation times, however, T_2 should increase with increasing mobility, which is inconsistent with the observed decrease of T_{2e} at increasing temperature. This indicates that the relaxating influence of water close to ^{31}P is relatively unimportant. Neither can $^{31}P-^{31}P$ dipolar coupling account for the observed relaxation, because for bacteriophage fd this type of coupling seems to cause the echo intensity to drop to e^{-1} of its initial value after 2.6 ms (22), which is long compared with the T_{2e} values found in our experiments. However, chemical shift fluctuations caused by motions can also spoil the refocussing of transversal coherence by π pulses and thereby shorten T_{2e} (23). For very slow motions such a mechanism would explain the observed T_{2e} trend (16). In the fast motion region, where T_{2e} increases as the motional frequency increases, the observed T_{2e} trend can only be the consequence of an increase of both motional amplitude and frequency together.

As the dynamic behavior of "naked" nucleic acids is already complex with a variety of internal motions taking place in a wide frequency range (24), the assumption of one single type of motion explaining all experimental ^{31}P data obtained for M13 and TMV is probably too simple. In fact, the absence of correlation between longitudinal and transversal relaxation as observed for M13 in our hybrid relaxation experiments and their different dependence on hydration suggest that T_1 and T_{2e} are governed by different types of independent motions. The relative similarity between spectra of 15 and 30% M13 gels in contrast with their large T_{2e} difference also indicates that lineshapes and transversal relaxation could well be dominated by different motions. A fact that further complicates the analysis of experimental results is that motional variations probably occur because of local viscosity variations within the gel and differences in local ^{31}P environments within the virion. Nevertheless, we have used the simple diffusion models for phosphorus mobility in M13 and TMV described in the pre-

vious paper (16) to interpret the experimental lineshapes and transversal relaxation decays in a more quantitative manner.

Isotropic diffusion

The combined effect of uncorrelated internal backbone motions and overall virion motions on ^{31}P NMR lineshapes and relaxation decays can be assumed to be roughly comparable to the effect of random ^{31}P diffusion in a viscous solution. This hypothesis was tested using the isotropic diffusion model discussed previously (16). For this type of diffusion, however, no echo lineshapes can be simulated that fit well to the experimental lineshapes of M13 and TMV. The relatively best, least-square fits for 15 and 30% M13 and 30% TMV are found for a diffusion coefficient of 6, 5, and 5 kHz, respectively (Fig. 1 *b*), but for these diffusion constants the simulated transversal relaxation is much too fast (Fig. 2 *b*). Clearly, the observed motional effects cannot be described by unrestricted, isotropic diffusion.

In the case of restricted motion, boundary effects become more significant as time increases. As a consequence, the isotropic diffusion model may provide a better description for the lineshape, defined by the quickly decaying free-induction decay, than for the relatively slow transversal relaxation. Therefore, neglecting T_{2e} anisotropy, we have also compared Fourier-transformed free-induction decays with the observed ^{31}P lines. Again, no lineshapes can be calculated that fit well to the experimental lineshapes. For TMV the simulated lineshape that relatively fits the best is the static lineshape (Fig. 1 *c*). Using the equation for ultraslow isotropic diffusion discussed previously (16), the observed relaxation curve can be reasonably simulated for a diffusion constant as small as 0.25 Hz (Fig. 2 *c*). For 15 and 30% M13 the relatively best fit is found for 3 and 4 kHz (Fig. 1 *c*). Once more, for these diffusion constants the simulated transversal relaxation is too fast (Fig. 2 *c*). Obviously, the isotropic diffusion model does not agree with the experimental data.

Rigid rod diffusion

By use of a uniaxial diffusion model, the hypothesis is tested that free or restricted rotation of the virions as rigid rods about their length axis explains both the observed motional lineshape narrowing and transversal relaxation. For several pairs of the diffusion coefficients D and restriction halfangles λ, lineshapes can be simulated that fit to the experimental lineshape of 15% M13 equally well. A good fit is produced by, for example, free rotor diffusion with a coefficient of 20 kHz, which seems to confirm an earlier suggestion (10), but the simulated T_{2e} (0.10 ms) for this case is lower than the experimental one (0.39 ms). The best fit to both the lineshape and the relaxation curve is found for a diffusion coefficient of 50 kHz and a restriction halfangle of 1.25 rad. For 30% M13 the experimental lineshape and transversal relaxation can hardly be interpreted consistently: the lineshape calculated for 0.75 rad and 200 kHz fits the best, but in this case the simulated T_{2e} value, 3 ms, is much too high. A reasonable fit to both the lineshape and the relaxation curve is produced by a diffusion coefficient of 40 kHz combined with a restriction halfangle of 1.0 rad. For TMV even the experimental lineshape alone cannot be simulated by use of the uniaxial diffusion model because of the sharp top in combination with the large linewidth in the lower part of the line. The most reasonable fit to both the lineshape and the relaxation curve is found for D = 25 kHz and λ = 0.7 rad.

Although in the highly viscous gels that we studied, the magnetic field is probably unable to orient the rod-shaped virus particles, we have also added partial orientation to the rigid rod model in an attempt to account for the inconsistency between lineshape effects and transversal relaxation. Indeed, as rotation about the magnetic field axis does not change the chemical shift, the net relaxation becomes slower for given D and λ, if the weight of parallel rod orientations is increased compared with an isotropic gel. For the same reason, however, motional narrowing also becomes less pronounced in the simulated spectrum. As a consequence, the experimental lineshapes and transversal relaxation decays still cannot be interpreted consistently in terms of rigid rod motion.

For rigid cylinders of the same dimensions as M13 and TMV, constants of 55 and 20 kHz can be calculated for unrestricted diffusion about the cylinder axis in pure water (25). These values almost equal the diffusion constants 50 and 25 kHz found above for 15% M13 and 30% TMV. This finding puzzled us, because gels of M13 and especially TMV are highly viscous: are translational and rotational diffusion in these concentrated gels governed by different viscosity parameters or do the high values of the simulated constants indicate collective motions of segments of the virus rather than rotation of the virus as a whole? The latter interpretation, however, is difficult to reconcile with the outcome of curvature studies, which show that M13 behaves as a rigid rod and not as a string of beats (26). Thus, although more successful than the isotropic diffusion model, the rigid rotor model fails to provide an unambiguous fit for 30% M13 and TMV, and the best diffusion constants that follow from the simulations are much higher than expected for viscous gels.

Combined diffusion

Instead of regarding M13 and TMV as rigid rods without internal mobility, we also considered the possibility that the nucleic acid backbone within the viruses undergoes restricted motion, superimposed on rotation of the virus particles as a whole. Such a picture is supported by the observation that motional narrowing is still prominently present in spectra of oriented solutions of bacteriophage fd, which is closely related to M13 (11). In the combined diffusion model used here, the internal motion is simpli-

fied to fast, restricted rotation about the length axis of the virus and the overall rotation is assumed to be unrestricted and very slow. Under these conditions the lineshape is dominated by the amplitude of the internal motion only, whereas transversal relaxation also reflects the influence of the overall diffusion (16). A good fit to the lineshape of 30% M13 is calculated for internal rotation with a restriction halfangle λ of 0.75 rad (Fig. 1 *e*). For λ kept at this value, the best fit to the experimental relaxation curve is calculated for an overall diffusion coefficient of D = 50 Hz (Fig. 2 *e*). Assuming first that hydration only influences the overall rotation of the virion, an attempt has been made to simulate the 15% M13 lineshape for λ = 0.75 rad as well. A good fit to the lineshape is obtained for D = 5 kHz, but the corresponding T_{2e} (0.16 ms) is too small. When λ is left free to vary, the best fit to both the lineshape and the relaxation curve of 15% M13 is obtained for λ = 0.9 rad and D = 400 Hz. For TMV the observed lineshape cannot be simulated well by use of the combined diffusion model. The relatively best fit to both the lineshape and the relaxation curve is found for λ = 0.6 rad and D = 3 Hz.

Despite this success in the simulation of M13 lineshapes, the treatment of the complicated backbone dynamics as simple uniaxial rotation is bound to be too simple. Diffusion models involving more angle fluctuations would probably result in smaller restriction angles per fluctuating angle than the λ values found above. This should be borne in mide when comparing the halfangles between 0.6 and 0.9 rad with, for example, backbone fluctuations of ±27° in the GHz range reported earlier for DNA (27). Interestingly, unoriented fd solutions show more motional narrowing than oriented ones at the same or even lower concentration (10, 11), which suggests that rotation about the length axis of fd does contribute a significant part to internal motion. That hydration influences both motional frequencies and amplitudes, as observed for M13, has been reported for DNA as well (24) and could be related somehow to the swelling of M13 upon hydration (2).

The low coefficients for overall diffusion as interpreted from the observed transversal relaxation better reflect the macroscopic viscosity of the virus gels than the values that followed from the rigid rod analysis above. Although the simulated decays fit well (Fig. 2 *e*), the observed decays still fit better to single exponentials (Fig. 2 *a*). This may be a consequence of the fact that the combined diffusion model neglects the exponential contribution of fast internal motions to transversal relaxation. In the T_{2e} region of interest such a contribution could only be significant for internal motions with frequencies $< 10^5$ Hz. Alternatively, the observed exponential deviation from the theoretical decays could be explained by local viscosity variations within the virus gels because of local hydration differences: contributions of more rapidly rotating virus particles would mask the nonexponential character of transversal relaxation close to t = 0.

Internal mobility variations

The impossibility to produce lineshapes that fit well the observed TMV line by use of the isotropic, rotor, or combined diffusion model has led us to include possible mobility differences among the three binding sites in TMV in our simulations. Using the fast diffusion model (16), a set of 10 lineshapes has been calculated for restriction halfangles λ being multiples of 0.15 rad up to 1.5 rad for every of the three sites separately. From the three sets 1,000 spectra were generated by making triple combinations. Comparing these combined spectra with the observed TMV spectrum, we generally found that a combination of two static sites and one mobile site greatly improved the lineshape fit. The best fit was produced by a λ value of 0.15 rad for site *1*, 1.5 rad for site *2*, and 0.3 rad for site *3* (as labeled by Stubbs and Stauffacher [13]; Fig. 1 *e*). Keeping this optimal combination of three halfangles λ fixed, the best fitting T_2 decay was calculated for overall diffusion with a coefficient of 3 Hz (Fig. 2 *e*). The model that sites *1* and *3* undergo only small amplitude motion, whereas site *2* is relatively mobile, is confirmed by NMR spectra of oriented TMV samples, in which the central resonance line is much broader than the other two (11) and by an early TMV model, on the basis of x-ray results, in which site *1* and *3* (labeled there as *2* and *3*) are in close contact with arginine residues (12). A recently refined model with two arginines binding site *1* and site *2* (28) would favor a combination of halfangles 0.15, 0.15, and 0.9 rad for sites *1*, *2*, and *3*, respectively, which fits to the observed lineshape almost equally well within experimental error.

Because of a slight, but systematic mismatch at the top between the experimental lineshape of 30% M13 and the best-fitting simulated lineshapes, we have tried to improve the lineshape fit for M13 assuming two ^{31}P fractions with different mobilities. Using the fast diffusion model, we calculated 10 spectra for λ values being multiples of 0.15 rad up to 1.5 rad and combined them in hundred pairs. For every pair the best bilinear fit to the experimental lineshape was calculated and the statistical variance was compared with the other bilinear fits. The best bilinear fit of all pairs to the lineshape of 30% M13, produced by a combination of 83% λ = 0.6 rad and 17% λ = 1.5 rad, reproduces the experimental lineshape very well indeed (Fig. 1 *e*). Keeping the fraction ratio fixed, we also find for 15% M13 that the lineshape is better described by a combination of 83% λ = 0.9 rad and 17% λ = 1.5 rad than by 100% 0.9 rad (Fig. 1 *e* and *d*, respectively). For these combinations of halfangles the best fits to the decays of 30 and 15% M13 are obtained for overall diffusion coefficients of 70 and 550 Hz, respectively (Fig. 2 *e*), which are slightly larger than the coefficients found for the single component model above.

When, in analogy with TMV, the immobile phosphorus fraction in M13 is associated with the phosphodiesters that interact most strongly with coat proteins, the percentage of 83% would indicate that per 10 monomers forming a unit cell of the protein coat, 20 out of 24 phosphodiesters are actually rigidly bound at a ratio of two nucleotides per monomer. The same stochiometry is suggested by the observation that during the extrusion of a completed virion out of the host cell every gene-5 protein molecule, which binds four nucleotides, is replaced by two gene-8 protein molecules (29). Interestingly, viral DNA that is twisted into a form resembling a double-stranded B-DNA helix with a pitch of 34 Å, a diameter of ~20 Å and 10 nucleotides per strand per turn, would fit in the hollow tube formed by the coat proteins with approximately the same protein/nucleotide ratio 1:2 and with the axial rise of about 3.4 Å per nucleotide observed in x-ray studies (4). Such a model seems to be confirmed by infrared linear dichroism results indicating a B-type backbone conformation as well (9). Perhaps the indications for maximal 20% A-DNA backbone in Raman spectra (8) and some regular DNA structure with a pitch of 27 Å in diffraction patterns (4) are related to the mobile fraction of 17% DNA found in our experiments.

Obviously, details of the tentative model of 83% viral DNA twisted into a sort of double-stranded B-helix should be specified in agreement with the experimental data reported until now. Raman spectroscopy has shown the sugar pucker to be C3′-endo, a feature of double-stranded A-DNA, rather than C2′-endo, typical for double-stranded B-DNA (8), but the absence of basepairing in the viral DNA could possibly allow such an A-type sugar puckering in combination with a B-type backbone. The different symmetries of the DNA helix and the protein coat would cause binding to distort the DNA backbone and destroy the equivalence among the phosphodiesters, which could offer a possible explanation for the absence of B-DNA backbone characteristics in diffraction patterns, Raman spectra, and NMR spectra. This would also explain the characteristics of a disordered DNA backbone found in ^{31}P NMR spectra of oriented and MAS samples in contrast to the case of, for example, TMV, where the RNA molecule and the protein share the same symmetry and as a consequence the ^{31}P NMR resonances of the three binding sites can be resolved. Backbone motions could further strengthen these features of disorder, especially under the high hydration conditions used for sample orientation, when the motional amplitudes tend to be large (see above).

CONCLUSION

In this paper we have shown by simulations that motional effects on ^{31}P NMR lineshapes and transversal relaxation of M13 and TMV cannot be described in terms of simple isotropic diffusion. The model for M13 diffusing as a rigid rod about its length axis is more successful for interpreting the NMR results obtained for 15% M13, although the diffusion coefficient, determined from the simulations, seems much higher than expected from the high viscosity of the gel. For 30% M13, however, the lineshape and transversal relaxation cannot be interpreted consistently and for 30% TMV the observed lineshape cannot even be simulated, indicating that the rigid rod model does not actually apply. Using a combined diffusion model, which assumes the lineshape to be dominated by fast internal DNA motions and transversal relaxation to reflect slow rotation of the virus as a whole, we can interpret the NMR results obtained for M13 in a consistent way. The diffusion coefficients for the slow overall diffusion are found to be low, as expected from the high sample viscosity. The restriction halfangle found for internal DNA motion indicates that the encapsulated DNA has substantial motional freedom. In contrast to simulations for M13, combined diffusion simulations fail to produce the experimental TMV lineshape. However, significantly improved lineshape fits are obtained for TMV under the assumption that the three binding sites have different mobilities. The finding that the best lineshape fits consist of one mobile and two static phosphodiesters seems to be confirmed by TMV models deduced from x-ray studies. Combined diffusion simulations with two components also improve the calculated lineshapes for M13. About 83% of the viral DNA appears to be rigidly bound at a protein/nucleotide ratio of 1:2. Together with the structural parameters of the protein coat this ratio suggests that despite the sugar pucker typical for A-DNA found by Raman spectroscopy, the backbone structure of 83% of the encapsulated DNA molecule may be roughly comparable to the backbone structure of double-stranded B-DNA, although binding to the protein coat probably induces significant distortions.

In this paper, parameters for ^{31}P mobility in M13 and TMV have been estimated by assuming motion and chemical shift anisotropy to be the only factors influencing the lineshape and transversal relaxation. Especially in the case of TMV, however, homonuclear dipolar coupling cannot be excluded as a significant contributor to the observed transversal relaxation (22). If this relaxation mechanism would be included in our simulation models, the resulting diffusion coefficients would be lower, but our limited experimental data do not allow such a refinement. Therefore, values of the diffusion coefficients presented in paper are safest when regarded as upper limits. As for the method of extracting motional parameters from experimental data by comparison with simulated data, our experience is that it is risky to analyze a NMR lineshape or a transversal relaxation decay alone. Both the lineshape and transversal relaxation

should be used to check motional models and obtain better estimations for the motional parameters.

We are grateful to Ruud Spruijt for isolation and purification of M13 and TMV, to Willem Stolp for lending us the fluoroptic thermometer, to Adrie de Jager and Lucie van de Steeg for experimental assistance, and to Ben Harmsen and Ruud Konings for helpful discussions.

This research was supported by the Netherlands Foundation of Biophysics with financial aid of the Netherlands Organization for Scientific Research (NWO).

Received for publication 30 November 1992 and in final form 11 February 1993.

REFERENCES

1. Rasched, I., and E. Oberer. 1986. Ff coliphages: structural and functional relationships. *Microbiol. Rev.* 50:401–427.
2. Dunker, A. K., R. D. Klausner, D. A. Marvin, and R. L. Wiseman. 1974. Filamentous bacterial viruses X. X-ray diffraction studies of the R4 A-protein mutant. *J. Mol. Biol.* 81:115–117.
3. Van Weezenbeek, P. M. G. F., T. J. M. Hulsebos, and J. G. G. Schoenmakers. 1980. Nucleotide sequence of the filamentous bacteriophage M13 DNA genome: comparison with phage fd. *Gene.* 11:129–148.
4. Banner, D. W., C. Nave, and D. A. Marvin. 1981. Structure of the protein and DNA in fd filamenous bacterial virus. *Nature (Lond.).* 289:814–816.
5. Marvin, D. A., R. L. Wiseman, and E. J. Wachtel. 1974. Filamentous bacterial viruses XI. Molecular architecture of the class II (Pf1, Xf) virion. *J. Mol. Biol.* 82:121–138.
6. Day, L. A. 1973. Circular dichroism and ultraviolet absorption of a deoxyribonucleic acid binding protein of filamentous bacteriophage. *Biochemistry.* 12:5329–5339.
7. Day, L. A., R. Wiseman L., and C. J. Marzec. 1979. Structure models for DNA in filamentous viruses with phosphates near the center. *Nucleic Acids Res.* 7:1393–1403.
8. Thomas, G. J., Jr., B. Prescott, S. J. Opella, and L. A. Day. 1988. Sugar pucker and phosphodiester conformations in viral genomes of filamentous bacteriophages: fd, If1, IKe, Pf1, Xf, and Pf3. *Biochemistry.* 27:4350–4357.
9. Fritzsche, H., T. A. Cross, S. J. Opella, and N. R. Kallenbach. 1981. Structure and architecture of the bacterial virus fd. An infrared linear dichroism study. *Biophys. Chem.* 283–291.
10. DiVerdi, J. A., and S. J. Opella. 1981. Phosphorus-31 nuclear magnetic resonance of fd virus. *Biochemistry.* 20:280–284.
11. Cross, T. A., P. Tsang, and S. J. Opella. 1983. Comparison of protein and deoxyribonucleic acid backbone structures in fd and Pf1 bacteriophages. *Biochemistry.* 22:721–726.
12. Stubbs, G., S. Warren, and K. Holmes. 1977. Structure of RNA and RNA binding site in tobacco mosaic virus from 4 Å map calculated from x-ray fiber diagrams. *Nature (Lond.).* 267:216–221.
13. Stubbs, G., and C. Stauffacher. 1981. Structure of the RNA in tobacco mosaic virus. *J. Mol. Biol.* 152:387–396.
14. Cross, T. A., S. J. Opella, G. Stubbs, and D. L. D. Caspar. 1983. Phosphorus-31 nuclear magnetic resonance of the RNA in tobacco mosaic virus. *J. Mol. Biol.* 170:1037–1043.
15. Hemminga, M. A., P. A. De Jager, J. Krüse, and R. M. J. N. Lamerichs. 1987. Magic-angle-spinning NMR on solid biological systems. Analysis of the origin of the spectral linewidths. *J. Magn. Reson.* 71:446–460.
16. Magusin, P. C. M. M., and M. A. Hemminga. 1993. A theoretical study of rotational diffusion models for rod-shaped viruses: the influence of motion on 31P NMR lineshapes and transversal relaxation. *Biophys. J.* 64:1851–1860.
17. Spruijt, R. B., C. J. A. M. Wolfs, and M. A. Hemminga. 1989. Aggregation-related conformational change of the membrane-associated coat protein of bacteriophage M13. *Biochemistry.* 28:9158–9165.
18. Slichter, C. P. 1978. Principles of Magnetic Resonance. Springer-Verlag. Berlin. 397 pp.
19. Eisenstadt, M. 1980. NMR hybrid relaxation methods of studying chemical, physical, and spin exchange. I. General theory and experimental methods. *J. Magn. Reson.* 38:507–527.
20. Snaar, J. E. M., and H. E. Van As. 1990. Discrimination of different types of motion by modified stimulated-echo NMR. *J. Magn. Reson.* 87:132–140.
21. Herzfeld, J., R. G. Griffin, and R. A. Haberkorn. 1978. Phosphorus-31 chemical-shift tensors in barium diethyl phosphate and urea-phosphoric acid: model compounds for phospholipid head-group studies. *J. Am. Chem. Soc.* 17:2711–2718.
22. Opella, S. J., and J. A. DiVerdi. 1982. Properties of the phosphodiester backbone of duplex DNA and filamentous bacteriophage DNA. *In* Biochemical Structure Determination by NMR. A. A. Bothner-By, J. Glickson, and B. D. Sykes, editors. Marcel Dekker, New York. 149–168.
23. Abragam, A. 1961. The Principles of Nuclear Magnetism. Oxford University Press, London. 599 pp.
24. Alam, T. M., and G. P. Drobny. 1991. Solid-state NMR studies of DNA structure and dynamics. *Chem. Rev.* 91:1545–1590.
25. Edsall, J. T. 1953. Size, shape and hydration of protein molecules. *In* The Proteins. H. Neurath, and K. Bailey, editors. Academic Press, Inc., New York. 549–686.
26. Song, L., U.-S. Kim, J. Wilcoxon, and J. M. Schurr. 1991. Dynamic light scattering from weakly bending rods: estimation of the dynamic bending rigidity of the M13 virus. *Biopolymers.* 31:547–569.
27. Hogan, M. E., and O. J. Jardetzky. 1980. Internal motions in deoxyribonucleic acid II. *J. Am. Chem. Soc.* 19:3460–3468.
28. Namba, K., R. Pattanayek, and G. Stubbs. 1989. Visualization of protein-nucleic acid interactions in a virus. Refined structure of intact tobacco mosaic virus at 2.9 Å resolution by x-ray fiber diffraction. *J. Mol. Biol.* 208:307–325.
29. Marvin, D. A., W. J. Pigram, R. L. Wiseman, E. J. Wachtel, and F. J. Marvin. 1974. Filamentous bacterial viruses XII. Molecular architecture of the class I (fd, If1, IKe) Virion. *J. Mol. Biol.* 88:581–600.